Crystal structure of a 3B3 variant—A broadly neutralizing HIV-1 scFv antibody

K. Reed Clark[1,2] and Scott T. R. Walsh[3]*

[1]Center for Gene Therapy, Nationwide Children's Hospital, Columbus, Ohio 43205

[2]Department of Pediatrics, College of Medicine, The Ohio State University, Columbus, Ohio 43210

[3]W. M. Keck Laboratory for Structural Biology, Center for Advanced Research in Biotechnology, University of Maryland Biotechnology Institute, Rockville, Maryland 20850

Received 14 August 2009; Revised 16 September 2009; Accepted 17 September 2009
DOI: 10.1002/pro.255
Published online 25 September 2009 proteinscience.org

Abstract: We present the crystal structure determination of an anti-HIV-1 gp120 single-chain variable fragment antibody variant, 3B3, at 2.5 Å resolution. This 3B3 variant was derived from the b12 antibody, using phage display and site-directed mutagenesis of the variable heavy chain (V_H) complementary-determining regions (CDRs). 3B3 exhibits enhanced binding affinity and neutralization activity against several cross-clade primary isolates of HIV-1 by interaction with the recessed CD4-binding site on the gp120 envelope protein. Comparison with the structures of the unbound and bound forms of b12, the 3B3 structure closely resembles these structures with minimal differences with two notable exceptions. First, there is a reorientation of the CDR-H3 of the V_H domain where the primary sequences evolved from b12 to 3B3. The structural changes in CDR-H3 of 3B3, in light of the b12-gp120 complex structure, allow for positioning an additional Trp side chain in the binding interface with gp120. Finally, the second region of structural change involves two peptide bond flips in CDR-L3 of the variable light (V_L) domain triggered by a point mutation in CDR-H3 of Q100eY resulting in changes in the intramolecular hydrogen bonding patterning between the V_L and V_H domains. Thus, the enhanced binding affinities and neutralization capabilities of 3B3 relative to b12 probably result from higher hydrophobic driving potential by burying more aromatic residues at the 3B3-gp120 interface and by indirect stabilization of intramolecular contacts of the core framework residues between the V_L and V_H domains possibly through more favorable entropic effect through the expulsion of water.

Keywords: HIV; envelope protein gp120; broadly neutralizing antibody; 3B3; single-chain variable fragment; X-ray crystallography

Introduction

Human immunodeficiency virus type-1 (HIV-1) quickly emerged as a global pandemic since its initial identification in the early 1980s and now infects more than 33 million people worldwide (World Health Organization HIV/AIDS website, http://www.who.int/hiv/en/). Approximately, 2 million people die annually from HIV-related causes (WHO, http://www.who.int/hiv/en/). Development of highly active antiretroviral treatment (HAART) has been successful in lowering HIV viral loads to undetectable levels and extending peoples' lives by more than 10 years providing patients strictly adhere to the prescribed daily dosing regimen. However, because of noncompliance, cost, availability, and the possibility of continual low-level viral replication, many patients (particularly in developing regions) relapse as HAART-resistant HIV escape mutants arise. Therefore, a preventative vaccine remains the best option to effectively limit the spread of HIV-1.

STRW dedicates this manuscript to Dr. Apostolos Gittis.

Grant sponsor: National Institutes of Health; Grant number: P01 AI056354.

*Correspondence to: Scott T. R. Walsh, Laboratory for Structural Biology, Center for Advanced Research in Biotechnology, University of Maryland Biotechnology Institute, 9600 Gudelsky Drive, Rockville, MD 20850.
E-mail: walshs@umbi.umd.edu

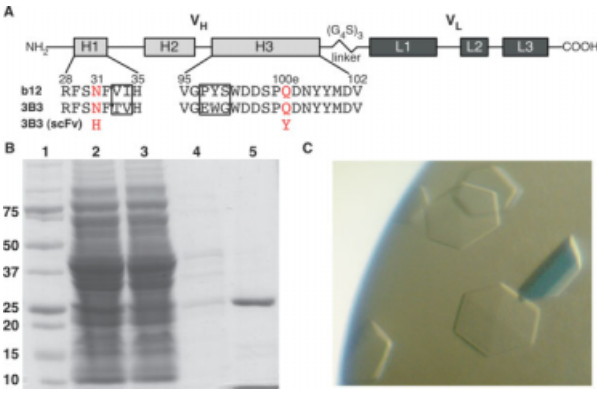

Figure 1. (A) Schematic diagram of the single-chain variable fragment (scFv) of 3B3. The variable heavy (V_H) and light (V_L) chains are connected together by a flexible glycine-serine linker. Primary sequence alignments are shown for the complementary-determining regions (CDR) of the V_H regions 1 (H1) and 3 (H3). Specific point mutations of the parent molecules of b12, 3B3 (Fab), and the 3B3 scFv variant are colored red. The boxed regions indicate the evolved sequence changes from b12 to 3B3 in the CDR walking phage display mutagenesis experiments.[12] (B) SDS-PAGE gel displaying the expression and purification of the 3B3 scFv. Lane 1 shows protein standards with molecular weights listed to the left in kDa. The subsequent lanes were of the periplasmic fraction from *E. coli* expression (Lane 2), the eluent during the loading of a protein L affinity column (Lane 3), a wash step from the protein L column (Lane 4), and finally the elution fraction of 3B3 from the protein L column (Lane 5). (C) Hexagonal- and trigonal-shaped protein crystals of 3B3 scFv.

Unfortunately, in light of the disappointing STEP trial data,[1] the possibility remains that active immunization as typically prescribed for other viruses might not be effective against HIV-1. Accordingly, there has been a refocusing of efforts to better understand HIV pathogenesis, correlates of protection, mechanism(s) of neutralization from a more basic research point of view in hopes of developing novel treatment strategies. We have championed an alternative vaccination approach using gene transfer of potent, preselected neutralizing antibody (NAb) genes that bypasses the need for active immunization.[2,3] The ultimate goal is to endow the host with protective circulating humoral immunity via adeno-associated virus (AAV)-mediated gene transfer before pathogen exposure.

A handful of broadly NAbs have been isolated directly from HIV patients using combinatorial phage display libraries of the patients RNA (reviewed in Ref. 4). These monoclonal antibodies target defined epitopes on the envelope glycoprotein (gp120 or gp41) on the surface of the HIV-1 virion. One such antibody, b12, targets the recessed CD4-binding site on gp120.[5] The binding epitope of b12 partially overlaps with the CD4-binding site thus blocking the initial viral gp120-host CD4 interaction and inhibiting viral fusion with the host cell membrane and infection.[6–10] b12 demonstrates broad, cross-clade neutralization of many divergent primary isolates.[11] Further binding optimization of b12 using complementary-determining region (CDR) walking and phage display mutagenesis resulted in an antigen-binding fragment (Fab) 3B3 that displayed enhanced binding affinity and neutralization of laboratory adapted and primary strains of HIV-1.[12] Figure 1(A) illustrates the substitutions in the CDRs of the variable heavy chain (V_H). In CDR-H1, residues V33 and I34 of b12 were selected for T33 and V34 in 3B3. In CDR-H3, residues P96, Y97, and S99 of b12 were selected for residues E96, W97, and G99 in 3B3. The sequence changes in 3B3 resulted in approximately eightfold higher binding affinities to various monomeric gp120s and ~3- to 54-fold enhancement in neutralization capacity depending on the HIV-1 subtype.[12] Further site-directed mutagenesis studies of the 3B3 CDR heavy and light chains generated a double mutation N31H/Q100eY variant of 3B3.[13] N31H/Q100eY-3B3 displays a ~23-fold lower IC_{50} than 3B3 in cell neutralization assays and approximately two-to threefold higher binding affinities (K_d) than 3B3 to different monomeric gp120s.[13]

Crystal structures have been determined for the unbound and bound states of b12. The structure of the unbound state of b12 was determined as a full IgG1κ antibody.[14] One bound state structure of b12 was solved as a Fab to a dimeric peptide mimotope.[15] For the other bound state of b12, the complex structure was determined using the Fab of b12 bound to a disulfide bond-stabilized gp120 core molecule.[10] The gp120 core molecule was engineered to adopt the conformation after it interacts with CD4 during the initial binding event by HIV. The unbound and bound structures of b12 superimpose with negligible differences between them indicating that no large conformational changes occur when b12 interacts with gp120 (there was a 2 Å change in one of the unbound Fab structures in comparison to the b12-gp120 structure). A surprising feature of the b12-gp120 complex structure revealed the paratope of b12 involved only residues of V_H CDRs interacting with gp120. No residues of b12 V_L CDRs make direct contact with the gp120 surface. This probably results from the evolution of the extra long 18-residue CDR-H3 that snakes it way to interact with the recessed CD4-binding site of gp120.[10] It should be noted that b12 was derived from phage display methods using RNA from cells of a long-term survivor HIV patient and that heavy chain only recognition of b12 to HIV gp120 may not occur *in vivo*. However, counterarguments have been presented on the validity of heavy chain only recognition of b12 (or similar antibody) to HIV *in vivo*.[16,17] One thing is certain with regards to HIV neutralization, antibodies that are raised to battle HIV infection have unique molecular recognition properties.

To date, we have successfully demonstrated that several broadly neutralizing human and nonhuman

Table I. *Crystallographic Parameters for the 3B3 scFv Structure*

Data collection	
Beam line	GM/CA 23ID-D
Wavelength	1.0332
Space group and unit cell (Å, °)	C2 $a = 199.2$, $b = 115.1$, $c = 92.4$, $\beta = 111.8$
Resolution (Å)	30–2.5 (2.6–2.5)[a]
No. of reflections	
Observed	61,604
Unique	22,816
Completeness (%)	92.3 (65.8)
Multiplicity	2.7 (1.5)
Mosaicity	0.53
Mean $I/\sigma I$	7.8 (1.7)
R_{merge}	0.12 (0.41)
Refinement	
Resolution (Å)	30–2.5
R_{cryst}	0.195
R_{free}	0.260
rmsd bonds (Å)	0.009
rmsd angles (°)	1.192
Protein atoms	11,301
Water atoms	275
Average *B*-factors (Å^2)	
Protein atoms (11,292)	24.6
Water atoms (275)	20.9
Ramachandran plot (%) (favored, allowed, outlier, disallowed)	95.5, 4.4, 0.1, 0.0

[a] Values in parentheses are for the highest resolution shell.

primate NAbs (b12, X5, and 3B3) can be produced *in vivo* from skeletal muscle of mice and rhesus macaques and secreted into the systemic circulation after rAAV gene transfer.[2,3,18] Once secreted, the animal's serum possesses anti-HIV-1 neutralizing activity. Moreover, stable serum levels have been observed for over a year in both mice and rhesus macaques. One potential challenge to this approach is whether therapeutic levels of NAbs are indeed achievable. To address this issue, we have optimized several variables for efficient antibody gene delivery and expression including: rAAV serotype, antibody genetic fusions for increased half-life, and inclusion of cis sequences for maximal expression.[2,18] This has resulted in increased antibody levels by greater than 100-fold over our initial efforts. Recent proof-of-concept data from our group demonstrated significant protection in rhesus macaques against a virulent SIVmac314 challenge using monkey neutralizing scFvs and a stabilized rhesus CD4-IgG immunoadhesin that incorporated the improvements mentioned earlier.[3]

To gain a stronger structural understanding of the enhanced binding affinities and neutralization capabilities of 3B3, we have determined the crystal structure of a single-chain variable fragment (scFv) N31H/Q100eY-3B3 variant to 2.5 Å resolution in the unbound state. Overall, the crystal structure of 3B3 superimposes well with the majority of the secondary structural elements of the unbound and bound states of b12 with two significant exceptions. There is minimal structural perturbation observed in the CDR-H1 in the vicinity of the N31H mutation of 3B3 in comparison to the b12 structures. The largest structural change involves a ~5-Å reorientation of the tip of the long CDR-H3 arm of 3B3 in comparison to the b12 structures. The final significant structural change of 3B3 in comparison with the b12 structures localizes to the packing environment around the Q100eY mutation in the CDR-H3. The Q100eY mutation of 3B3 triggers a secondary structure change of CDR-L3 of the V_L domain from a type I′ turn seen in the b12 structures to a turn with type II′ character. The consequences of these structural changes in 3B3 result in more intramolecular hydrogen bonds among residues and fewer water-mediated hydrogen bonds at the V_H-V_L interface in comparison to the b12 structures. Thus, the enhanced neutralization capabilities and binding affinities of N31H/Q100eY-3B3 scFv probably result from a higher hydrophobic driving force of the selected aromatic residues (N31H in CDR-H1 and Y98W and Q100eY in CDR-H3) at the binding interface with gp120 and a stabilization of framework residues among CDR-H3, -H2 β-sheets, and -L3 at the V_H-V_L interface.

Results

3B3 scFv preparation

A bacterial expression system was constructed to express the 3B3 scFv into the periplasmic space of *E. coli*. The expression vector consists of an alkaline phosphatase promoter followed by a modified custom signal sequence for localization into the periplasm through the Sec transport machinery. The signal sequence consists of MKKNIAVVVVVVVVVVIAT NAMA and engineered from the signal secretion determinants deciphered by the Silhavy and coworkers.[19] Expressed 3B3 was isolated from the periplasmic space of *E. coli* cells and purified to homogeneity using protein L affinity chromatography [Fig. 1(B)]. Typical 3B3 protein yields were 1.4 mg L^{-1} of culture.

Crystallization and structure determination

The 3B3 scFv crystallized as either hexagonal- or trigonal-shaped plates from PEG-8000 under slightly acidic conditions [Fig. 1(C) and Material and Methods]. A 3B3 protein crystal diffracted greater than 2.5 Å resolution and indexed to the monoclinic space group C2. Cell content analysis indicated six 3B3 copies within the asymmetric unit with a Matthew's coefficient (V_M) of 3.1 and solvent content of 60%. The 3B3 structure was solved using molecular replacement by searching for six copies of the V_H and V_L domains from the b12-gp120 complex structure (2ny7.pdb[10]) using the program Phaser.[20] The 3B3 structure was refined to a R_{cryst} and R_{free} value of 0.195 and 0.260, respectively. The average crystallographic *B*-factors were 21.5, 20.7,

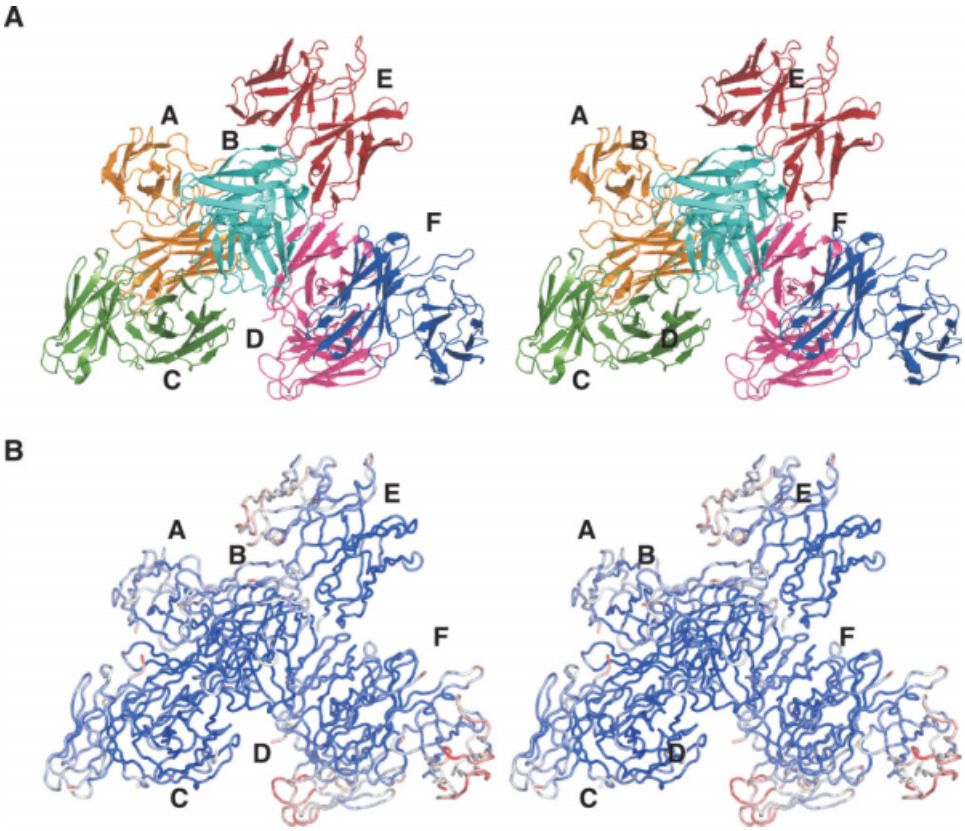

Figure 2. (A) Stereo ribbon diagram displaying the packing interactions among the six molecules of the 3B3 scFv within the asymmetric unit cell. Each 3B3 chain is labeled and colored differently. (B) Stereo view as in (A) of the six molecules of the 3B3 scFv colored as a gradient from blue-white-red indicating increasing values of the temperature *B*-factors.

21.3, 29.0, 26.1, and 30.0 $Å^2$ for chains A–F, respectively. Crystallographic and structural parameters are listed in Table I.

3B3 scFv structural description

Within the crystallographic asymmetric unit, six independent 3B3 chains were built into the electron density map with varying degrees of completeness (Fig. 2). Noncrystallographic symmetry (NCS) was not used as restraints during structure refinement. The N-terminal six-residue histidine tag was not observable in the electron density for any of the chains and the chains began with Q7 besides chain C, which was modeled as an Ala. Electron density allowed building of the Gly_4Ser linker connecting V_H to V_L domains for chain B up to G137. The other 3B3 chains end at S133 besides chain A, which was only modeled to S132. For the V_L domains, the chains began again at either S148 (chain C) or E149 (chains A, B, and D–F) and terminated at either R255 (chains A and D–F) or K256 (chains B, C). Figure 2(B) highlights regions of increased mobility as indicated by higher temperature *B*-factors. Higher *B*-factors cluster to termini residues and the loop regions including the CDRs of the V_H and V_L domains.

The individual chains of 3B3 display an overall similarity at the backbone level. Table II lists the pairwise root mean square deviations (rmsds) for backbone superimpositions (233 C_α atoms) for all the chains. Besides rotamer differences between the individual chains of 3B3, the structures superimpose with each other with an average rmsd of 0.28 Å for the Cα atoms indicating no large conformational changes among the six individual 3B3 chains in the asymmetric unit. Figure 3(A) illustrates the backbone superimpositions of each of the chains onto chain A. Chain A was used for the superimpositions because the electron density allowed for the most complete model tracing involving the CDR loops and will be used for further

Table II. *Root Mean Square Deviations for Backbone Superimpositions for Each 3B3 Chain*[a]

Chain	A	B	C	D	E	F
A	–					
B	0.184	–				
C	0.209	0.213	–			
D	0.282	0.277	0.286	–		
E	0.299	0.299	0.320	0.281	–	
F	0.323	0.335	0.316	0.278	0.341	–

[a] The backbone Cαs were used for the superimpositions and reported in Å.

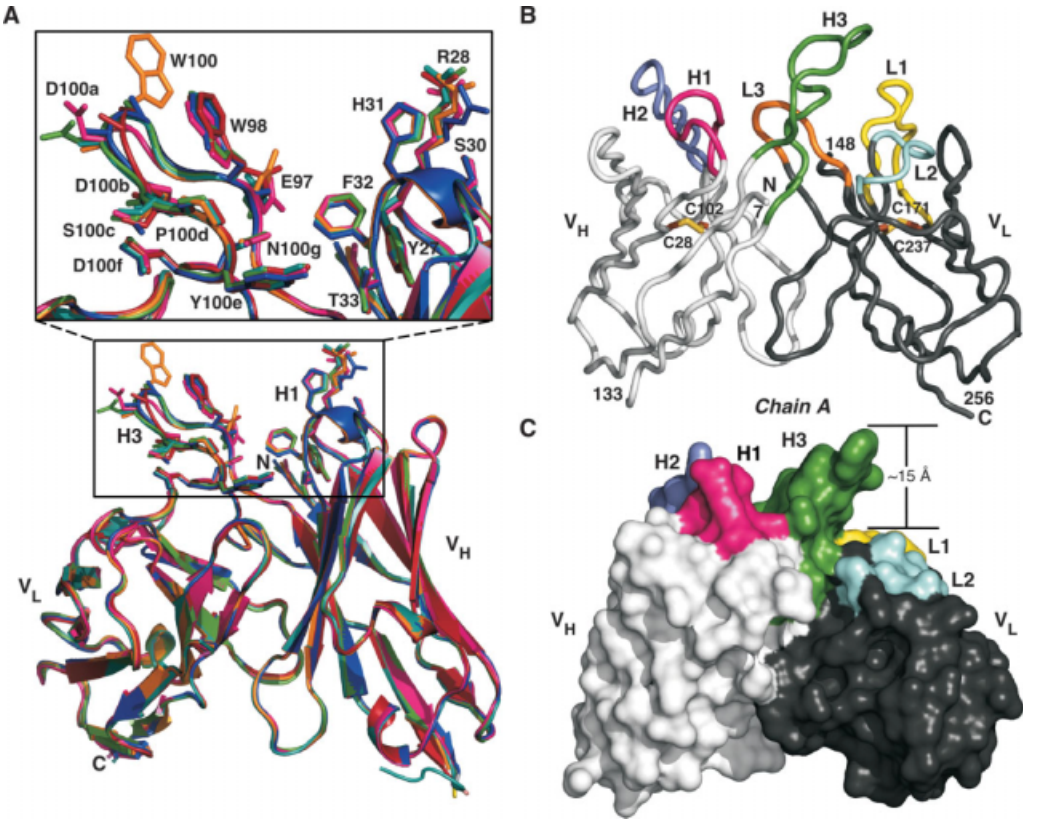

Figure 3. (A) 3B3 backbone Cα superimpositions of each chain onto chain A. The secondary structural elements were used for the backbone superimpositions. Each chain is colored identically as in Figure 2(A). The zoomed inset depicts the CDR-H1 and the tip of the long finger CDR-H3. Side chains of the residues of the CDRs are shown as sticks. (B) Structural cartoon of chain A of 3B3 with each of the six CDR regions colored separately of the V_H and V_L domains. The V_H and V_L CDRs are labeled H1, H2, H3, L1, L2, and L3, respectively. The V_H and V_L domains each contain a single disulfide bond depicted as brown and yellow sticks and labeled. (C) Molecular surface representation of chain A of 3B3 and colored as in B. The distance from W100 side chain to base of the 3B3 is ~15 Å.

structural comparisons discussed later. A cartoon ribbon representation for chain A of the 3B3 is illustrated in Figure 3(B) with the CDRs colored individually. A characteristic feature of 3B3 and its parent molecule, b12, involves a long 18-residue CDR-H3, which extends ~15 Å from the base of the CDR surface [Fig. 3(C)]. At the tip of CDR H3, a critical tryptophan residue (W100) plays an essential role in the binding interaction with gp120 (discussed later).[9] Only the electron density around chain A allowed building for the complete side chain of W100 (Fig. 4), whereas the other chains were modeled as an Ala for W100. For CDR-H3 of chain E, there is a maximum 1.5 Å displacement between the alpha carbons of A111 of chains A and E. However, no peptide bond flips were observed in this region of the CDR-H3 of chain E in relation to the other chains.

3B3 structural comparison to the b12 structures

Figure 5 illustrates the backbone superimpositions of the V_H-V_L domains using secondary structural elements of 3B3, unbound b12, and bound b12-B2.1 peptide structures onto the b12-gp120 complex structure. Chain A of 3B3 superimposes with a backbone rmsd of 0.59 Å (232 C_α positions). The other chains of 3B3 in the asymmetric unit display similar backbone rmsd values. Both V_H-V_L domains of the unbound b12 IgG1 structure superimpose onto the b12-gp120 bound structure with rmsds of 0.34 Å (232 $C_{\alpha s}$). In addition, both V_H-V_L domains of the bound b12-B2.1 peptide mimotope structure (2 b12 Fabs in the asymmetric unit) superimpose onto the b12-gp120 bound structure with an average rmsd of 0.40 Å (232 $C_{\alpha s}$). Independently, all the chains of 3B3 superimpose onto either V_H-V_L domains of the unbound b12 IgG1 structure with backbone rmsds of ~0.58 Å similar to the 3B3-b12 bound superimposition. Thus, at least at the secondary structure and domain levels, 3B3 displays no large conformations changes between the free and bound states of b12. Furthermore, there are no large conformational changes between the unbound and bound states of b12.

The *in vitro* evolution of b12 to 3B3 that occurred using phage display mutagenesis involved residues in CDR-H1 and -H3. In Figure 5(A), CDR-H1 is displayed for three structures (b12 unbound (chains K and M) and bound to gp120 and 3B3). The overall CDR-H1 backbone geometries remain relatively constant among

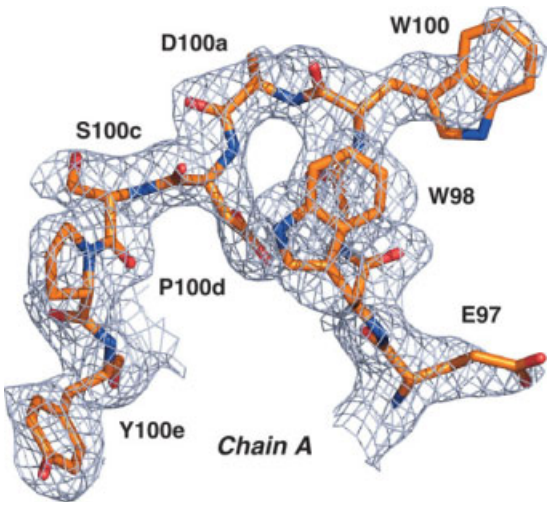

Figure 4. Simulated annealed σ_A-weighted omit electron density map (light blue) contoured at 1.0σ for the modeled CDR H3 tip for chain A.

the three structures displayed in Figure 5(A) as well as the other b12 unbound Fab (chains H and L) and b12-B2.1 bound structures, with structural changes occurring at the side-chain levels. The CDR-H1 region in the b12-gp120 complex structure buries ~269 Å^2 surface area (recalculated using Pisa). An unique feature in the b12-gp120 complex structure involves interactions of R28 of b12, which is not part of the canonical CDR-H1, with gp120. In the b12-gp120 complex structure, the guanidinium side chain of R28 was modeled as two rotameric states with both states forming multiple intermolecular hydrogen bonds with main-chain and side-chain groups of gp120. The side chain of R28 of the b12 free structure is rotated back toward CDR-H1 region away from the gp120 binding surface, whereas the side chain of R28 in the 3B3 structure is positioned in between the two conformations seen in the b12-gp120 complex structure. In the current state, the side chain of R28 of 3B3 would clash with gp120 residues. The side chain of R28 of both 3B3 and unbound b12 would only have to undergo side-chain rotamer flipping to adopt the conformations observed in the b12 bound structure requiring minimal energetic cost.

Moving to N31, in the b12-gp120 complex structure the side-chain carbonyl group of N31 forms an intramolecular hydrogen bond with the side-chain hydroxyl group of S30 (2.9 Å), and the side-chain amino group of N31 forms an intermolecular hydrogen bond with backbone carbonyl of S365 O of gp120 (3.0 Å). In addition, N31 buries ~80 Å^2 of surface area at the b12-gp120 interface (second largest burial only to R28, which buries the largest amount of surface area with 129 Å^2). The intramolecular hydrogen bond between N31 and S30 of CDR-H1 seen in the b12-gp120 complex structure is not conserved in the unbound b12, bound b12-B2.1, or 3B3 structures. In the unbound b12 structure, the side chain of N31 is rotated away and potentially only in hydrogen bonding distance when bound to gp120. In the 3B3 structure, this position is mutated from an Asn to a His and the aromatic side chain of H31 overlays reasonable well with the side chain of N31 from the bound b12-gp120 structure. However, the Nδ1 of H31 of 3B3 is too far away to form an intramolecular hydrogen bond with S30 Oγ (3.7 Å). All three structures come pack into side-chain register at F32, which packs over the N-terminal portion of the CD4 binding loop (β_1-α_3) of gp120.

In comparing CDR-H2, 3B3 and the unbound b12 structures superimpose with negligible rmsds at both the backbone and side-chain levels with the bound b12-gp120 and b12-B2.1 structures. 3B3 and b12 have identical primary sequences for CDR-H2. The bound b12-gp120 structure buries ~314 Å^2 of surface area with residues CDR-H2 of N52 and Y53 forming two intermolecular hydrogen bonds with gp120 residues of the CD4-binding loop and β20/21. There are no significant conformational changes observed for CDR-H2 going from the unbound to bound states of b12 and most likely for the 3B3 bound state, because its CDR-H2 adopts a similar conformation as seen with b12-gp120 complex structure.

Figure 5(B) highlights the tip of the CDR-H3 displaying the three structure superimpositions of b12 unbound (chains K and M), b12 bound to gp120, and 3B3. The extra long 18-residue CDR-H3 of b12 makes extensive contacts with gp120 burying 348 Å^2 of surface area docking onto the CD4-binding site of gp120. The indole side chain of W100 of b12 wedges itself between cavity formed by R419, N386, and the N-linked glycan of N386 of gp120. W100 O forms a hydrogen bond with R419 Nη1 of gp120 (2.6 Å). The *N*-acetylglucosamine (NAG 886) O6 atom attached to N386 of gp120 forms a hydrogen bond to the main-chain nitrogen of W100 of b12 (3.3 Å) in a rare glycosylation-mediated antigen–antibody interaction. The Y98 Oη of b12 forms a potential long hydrogen bond to R419 Nη1 of gp120 (3.6 Å). Chains H and L of one of the Fab arms of the unbound b12 structure display a maximum 2.0 Å backbone displacement for the tip of the CDR-H3 in comparison with the b12-gp120 structure (Fig. 5, gray structure). On the other hand, chains K and M of the other Fab arm of the unbound b12 structure in comparison to the b12-gp120 complex structure display negligible backbone atom displacements with differences arising with the side-chain rotamers (e.g., W100 in the b12 structures). The N-terminal end of the CDR-H3 of 3B3 adopts a wholly different main-chain conformation in comparison to the b12 structures (including the b12-B2.1 bound structure). The structural changes seen in 3B3 appear precisely where the amino acid changes occurred during the *in vitro* phage display experiments with b12. The sequence changes from Pro-Tyr-Ser in b12 to Glu-Trp-

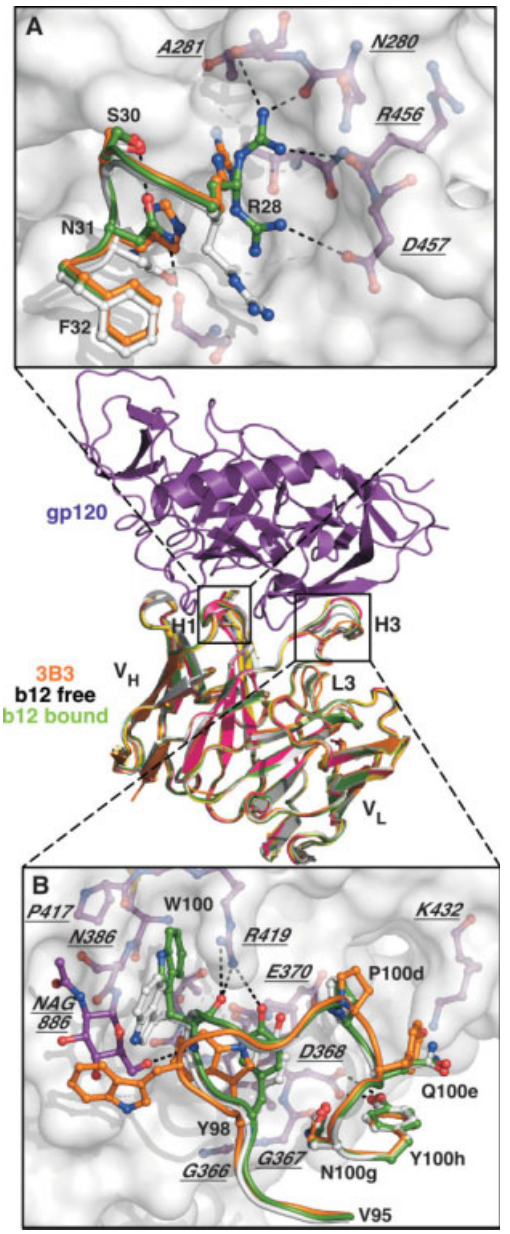

Figure 5. Structural comparison among the 3B3 scFv to the unbound state of b12 IgG1 (1hzh.pdb[14]), bound state of the b12 Fab to a B2.1 peptide mimotope (1n0x.pdb[15]), and the bound state of b12 Fab to the HIV-1 gp120 coat protein (2ny7.pdb[10]). The structures are colored purple, yellow, pink, white, gray, orange, and green for gp120, b12-B2.1 (chains K/M), b12-B2.1 (chains H/L), b12 unbound (chains K/M), b12 unbound (chains H/L), 3B3 (chain A), and b12-gp120, respectively. The 3B3 and b12 (unbound and B2.1 bound) structures were superimposed onto the bound b12-gp120 structure using the Cα atoms of the secondary structural elements of the V_H and V_L domains. (A) Expanded region of the CDR-H1 interactions with gp120. Hydrogen bonds between b12 and gp120 are shown as black dashes. The b12 residues are labeled and the gp120 residues are italicized and underlined. (B) Expanded region of the tip of CDR-H3 interactions with gp120. The expanded structural views have been rotated and only the b12 unbound (chains K/M), 3B3, and b12-gp120 bound structures are displayed for visual clarity.

Gly in 3B3 [Fig. 1(A)]. The main chain of CDR-H3 of 3B3 deviates from the b12 structures starting at E97/P97 (3B3/b12 residue) and superimposes well again starting at residue D100b (3B3 and b12 residue). There are distance changes from ~2.0–6.0 Å among the corresponding W100 Cα atoms of 3B3 and the five b12 structures (Fig. 5).

At the C-terminal end of the CDR-H3 of 3B3, a single point mutation was introduced by changing Q100e to a Tyr (this mutation in context of a scFv architecture showed enhanced binding affinity to gp120 and neutralization capability to primary HIV-1 isolates).[13,21] The side-chain residues between Y100e in 3B3 and Q100e in b12 display negligible rmsds out to the Cγ atoms. Surprisingly, the Q100eY mutation of 3B3 alters the loop conformation of CDR-L3 that packs against CDR-H3 at the V_H-V_L interface in comparison to the five b12 structures (Fig. 5). As noted previously, the residues of the V_L CDRs do not make direct contact in the b12-gp120 complex structure. Figure 6 displays the 3B3 and b12 complex structures centered on 100e (CDR-H3) and CDR-L3. Replacement of Q100e with a Tyr removes an intramolecular hydrogen bond of 2.8 Å between Q100e Oε1 (CDR-H3) and A93 N (CDR-L3), which links these two CDRs in the b12 structures. The loss of this hydrogen bond in 3B3 triggers two peptide bond flips at G92 and A93 altering the CDR-L3 turn geometry relative to the b12 structures. The dihedral angles of G92-A93-S94 alter from ε-α_L-α_L conformations in the b12 structures to β-α-α conformations in 3B3 (Table III). There is a maximum displacement of 5.6 Å between the carbonyl groups of A93 of 3B3 and the b12 structures. The CDR-L3 conformations observed in either 3B3 or b12 structures do not adopt any canonical Vκ loop conformations.[22,23]

The Q100eY mutation in 3B3 from b12 alters the local hydrogen bonding network around the CDR-L3 region (Table III). For residues Y91–Y96 of CDR-L3, six intramolecular hydrogen bonds were observed in 3B3, whereas in b12 there were only four hydrogen bonds. In the b12-gp120 complex structure, there were an additional six water-mediated interactions in this region. In the 3B3 structure, three (chains A and B) to four (chain B) water-mediated interactions were observed between the nitrogen backbone and/or serine side chain of A93, S94, and S95. No water-mediated interactions were observed for chains C, D, and F of 3B3. In both 3B3 and b12 structures, Y91 Oη forms a hydrogen bond to V_L G50 N (2.8 Å in 3B3 and 3.0 Å in b12), Y91 N forms a hydrogen bond to V_L R32 O (3.0 Å in 3B3 and 3.3 Å in b12), and Y91 O hydrogen bonds to V_L R32 Nε in 3B3 (3.1 Å) and to Wat170 in b12 (3.2 Å). In comparison to the b12 structures, there is a loss of the β-turn hydrogen bond between G92 O and S95 N in 3B3, but G92 O forms a new short hydrogen bond with the Y96 Oη side chain (2.6 Å). The carbonyl group of 3B3 A93 forms a bidentate

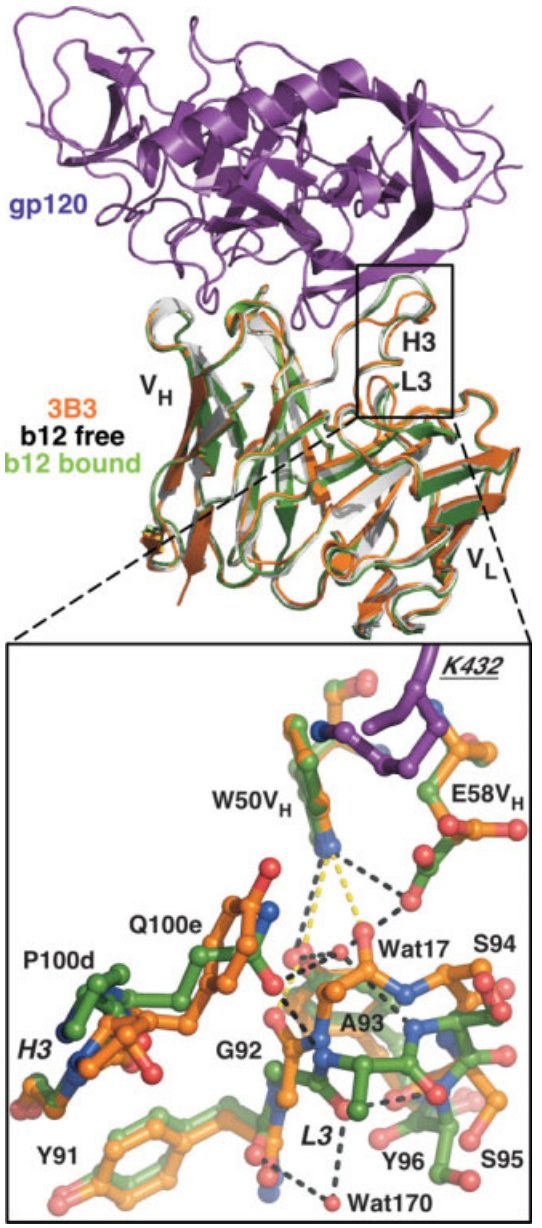

Figure 6. Structural comparison between the 3B3 scFv and the bound state of b12 Fab to the HIV-1 gp120 coat protein highlighting the backbone and side-chain changes observed between the CDR-H3 and framework regions of the two structures. The structures are colored as defined in Figure 5. For clarity, the zoomed region only displays the 3B3 scFv and b12 bound structures and rotated to highlight key features. The b12 unbound (both Fabs) and b12-B2.1 structures (both Fabs) look similar to the b12-gp120 bound structure. In addition, the water-mediated interactions between the nitrogen backbone groups of A93-S95 to Wat42 are not displayed for clarity, but are listed in Table III.

hydrogen bond with Y96 Oη (3.1 Å, V_L) and W56 Nε1 (3.1 Å, V_H). A93 O of b12 formed a hydrogen bond with Q100e Oε1 (2.8 Å). In the b12 structures, a water molecule (Wat17) coordinates four interactions between side and main atoms among CDRs H3, L3, and V_H β-sheet residues. The altered CDR-L3 confirmation displayed by 3B3 replaces the interactions seen with Wat17 in b12 with specific main-chain and side-chain hydrogen bonds discussed in detail later.

Discussion

The major question that this study aims at answering involves what structural features of 3B3 give rise to its higher binding affinities and neutralization capabilities to gp120 variants relative to its parent molecule, b12. Although it would be ideal to have the 3B3-gp120 complex structure for direct comparison, the unbound 3B3 structure provides unique insights into the evolution of broadly NAbs to the HIV-1 gp120 antigen. The *in vitro* evolution of b12 from the 1994 study involved phage display mutagenesis of positions 31–35 of CDR-H1 and positions 97–100 of CDR-H3.[12] The structural comparisons of 3B3 with the b12 unbound and bound states along with previous mutagenesis data lead us to speculate that the enhanced binding affinities and neutralization ablities of 3B3 arise from higher hydrophobic driving potentials between interfacial contact residues with gp120 and by stabilization of the V_H-V_L interface of the antibody. Stabilization of the V_H-V_L interface of 3B3 may result from more favorable hydrogen bonding of interfacial residues, a larger surface area burial of residues at the interface, a larger favorable entropic force through the removal of water at the interface, or combinations of these factors. We go through an analysis with the new 3B3 structure with previous data and highlight specific key points that lead to our conclusion.

In the original 1994 article describing the evolution of b12, CDR-H1 displayed a primary sequence preference for an Asn at position 31, an aromatic residue at position 32, a Ser or Thr at position 33, a hydrophobic residue at position 34, and a hydrophobic and/or aromatic residue at position 35.[12] The b12 CDR-H1 sequence is N-F-V-I-H. The 3B3 CDR-H1 sequence is N-F-T-V-H [Fig. 1(A)]. The 3B3 sequence would potentially lead to an Asn-linked glycosylation site at N31 (sequence motif of Asn-X-Ser/Thr, where X is any amino acid besides Pro). Therefore, further CDR walking phage display mutagenesis experiments were performed by Barbas and coworkers. Sequence selection demonstrated a preference for a His at position 31 that displayed approximately three- to fourfold enhanced binding affinity to monomeric gp120 and removed the potential of an Asn-linked glycan at position 31.[21] The CDR walking mutagenesis, binding and neutralization studies were performed as Fab architectures expressed and purified from *E. coli*, therefore generating unglycosylated Fabs. Further site-directed mutagenesis studies in context of a scFv of 3B3 fused to an immunotoxin of a truncated form of Pseudomonas exotoxin A, indicated a approximately twofold increase in IC_{50}s of cytopathic activities against Env-

Table III. *Dihedral Angles, Accessible Surface Areas, and Intramolecular Contacts for the CDR L3 of 3B3 and b12*[a]

Residue	ϕ,ψ (3B3)	ϕ,ψ (b12)	ASA[b] (3B3)	ASA (b12)
V90	−105, 124	−102, 145	10	5
Y91	−119, 169	−142, 161	5	53
G92	−177, −149	89, 157	57	15
A93	−86, −47	51, 48	38	79
S94	−126, 4	66, 3	70	112
S95	−144, 140	−108, 91	66	39
Y96	−142, 129	−117, 112	12	146
			Distance (Å)	
3B3 chain A hydrogen bonds[c]				
Y91 N V_L – R32 O V_L			3.0	
Y91 O V_L – R32 Nε V_L			3.1	
Y91 Oη V_L – G50 N V_L			2.8	
G92 O V_L – Y96 Oη V_L			2.6	
A93 O V_L – Y96 Oη V_L			3.1	
A93 O V_L – W50 Nε1 V_H			3.1	
3B3 water-mediated interactions				
A93 N V_L – Wat42			3.2	
S94 N V_L – Wat42			3.1	
S95 N V_L – Wat42			3.2	
S94 Oγ V_L – Wat 123 (chain B only)			3.2	
b12 hydrogen bonds				
Y91 N V_L – R32 O V_L			3.3	
Y91 Oη V_L – G50 N V_L			3.0	
G92 O V_L – S95 N V_L			3.0	
A93 N – Q100e Oε1 V_H			2.8	
b12 water-mediated interactions				
E58 Oε2 – Wat17			2.6	
S94 N VL – Wat17			3.2	
Y96 Oη – Wat17			2.6	
Q100e Oε1 – Wat17			3.0	
Y91 O V_L – Wat170			3.2	
G92 O V_L – Wat170			2.8	

[a] Values are reported for the b12-gp120 complex structure.
[b] Accessible surface area calculations were performed using Pisa.
[c] Hydrogen bonds are listed for distances ≤3.3 Å.

expressing cells with the N31H single mutation (IC_{50} = 5.7 ng mL^{-1}) relative to wild-type (wt) 3B3 (IC_{50} = 2.5 ng mL^{-1}).[13] In the b12-gp120 structure, the side chain of N31 of b12 forms an intramolecular hydrogen bond between the carbonyl group and the side chain of S30 V_H, and the side-chain amino group of N31 forms an intermolecular hydrogen bond with the backbone carbonyl of S365 of gp120. The 3B3 (N31H, Q100eY) scFv structure maintains a similar conformation as seen with the b12-gp120 structure displaying a potential intramolecular hydrogen bonding distance to S30 and probably enhanced packing interactions of 3B3 with gp120 through stronger van der Waals interactions with an aromatic residue of His at position 31 resulting in the higher binding affinity changes of 3B3 (N31H, Q100eY) scFv over b12.

In the CDR-H1, b12 evolved from a Val-Ile at positions 33 and 34 to a Thr-Val in 3B3.[12] These main-chain and side-chain conformations in the 3B3 structure overlay completely with all five b12 structures (data not shown). Extensive phage display mutagenesis of CDR-H1 demonstrated a clear preference for a Thr at position 33.[21] Binding affinity data showed a approximately three- to fourfold improvement with a Thr at position 33 for 3B3 over a Val for b12, but this sequence tested also contained the N31H mutation described earlier. Analysis of the 3B3 structure indicates that the side-chain carbonyl of T33 is within intramolecular hydrogen bonding range with Y100h Oη of CDR-H3 (3.2 Å). Furthermore, an intermolecular hydrogen bond may exist between T33 Oγ1 and D368 Oδ1 of gp120 (3.6 Å away) providing a structural rationale for the selection preference of a Val for a Thr at position 33 and the binding enhancement observed for 3B3 relative to b12.

The major enhancement in binding affinity and neutralization ability to gp120 from b12 to 3B3 occurred at the N-terminal end of CDR-H3.[12] Mutations in the CDR-H3 loop play a dominating role in the generation of NAbs to HIV and other viral antigens.[17,24] The sequence of b12 is Pro-Tyr-Ser for positions 97–99 of CDR-H3. The sequence of 3B3 is Glu-Trp-Gly for these positions. Chain shuffling and further CDR walking phage display mutagenesis studies clearly demonstrated a preference of either Glu-Trp-Thr or Glu-Trp-Gly for positions 97–99, as seen in 3B3, with approximately eightfold increase in binding affinity to monomeric gp120 over b12 (measured as

purified Fabs).[16,21] In context of a 3B3 scFv framework, inclusion of a Glu-Trp-Gly sequence at positions 97–99 displayed the same fivefold increase in binding affinity to various monomeric gp120 sequences over the Pro-Tyr-Ser sequence in b12.[13] In comparing the 3B3 and b12 structures, this is one of the regions that exhibited the largest conformational change. Larger CDR H3 loop conformational changes have been observed for a gp120 coreceptor binding antibody, X5, which demonstrated a 17 Å change of the CDR-H3 from the unbound[25] to bound[26] states of X5. At the apex of CDR-H3 in both 3B3 and b12 is W100. Trp100 in these antibodies is essential for the interaction with gp120. Mutation of W100 to Ala abrogates all binding affinity to gp120.[27] The side chain of W100 positions itself into a pocket created by main-chain residues of gp120 and side chain of R419 of gp120 [Fig. 5(B)]. Another crucial residue of the b12 paratope to gp120 is Y98. As seen with the W100 to Ala mutation, Y98A of b12 also abolishes binding to gp120.[9] The side chain of Y98 forms extensive van der Waals contacts over P369 of gp120 (Y98 buries ~100 Å^2 of surface area) and forms a potential long hydrogen bond between Y98 Oη and R419 Nη1 of gp120 (3.6 Å).

Comparison of the 3B3 structure to both b12 structures indicates a potential change in the binding mode of the CDR-H3 from a "lock-and-key" mechanism for b12 to an "induced-fit" mechanism for 3B3 when interacting with gp120. Ideally, we would have the 3B3-gp120 crystal structure for direct comparison with the 3B3 unbound structure. Nevertheless, this hypothesis is supported by several observations. The unbound b12 structure superimposes with negligible rmsds with the bound b12 structure indicating that binding to gp120 induces no large conformational changes in the b12 structure. This behavior is typical of structures of affinity-matured antibodies with and without antigen [Fig. 5(B)].[28] There are several side-chain rotamer changes that take place between the unbound and bound structures of b12. For example, the side chain of W100 of CDR-H3 only needs to change its χ^1 angle from the unbound b12 structure to adopt the conformation in the bound b12-gp120 structure. These side-chain rotamer changes between the V_H CDRs of the b12 structures would require minimal energetic costs. Furthermore, model building of the CDR-H3 loops for both b12 crystal structures displayed clear electron density to trace all the main-chain and side-chains groups, and these regions refined with relatively low temperature *B*-factors indicating overall restricted mobility.

We speculate that mutation of P97 to a Glu in 3B3 is responsible for the change in binding mechanism for the CDR-H3 loop. P97 of the b12 structures locks the N-terminal end of the CDR-H3 in place through its trans dihedral conformation providing a means of enhanced rigidity for this extra-long 18-residue CDR-H3. Mutation of P97 to a Glu as in 3B3 removes the limited angular geometry of a Pro with a more flexible residue of a Glu. The structure of 3B3 displays higher mobility in the CDR-H3 regions, mostly at the side-chain level because the backbone density was clear for chain tracing, for the six chains built into the electron density as assessed by higher than average refined temperature *B*-factors. In fact, several of the side chains of CDR H3 were modeled as alanines including the critical hot-spot residue W100 with the exception of chain A.

The amino acid substitutions at the N-terminal region of the CDR-H3 of 3B3 would appear to make enhanced interactions with the gp120 relative to b12. For 3B3, the tip of the CDR-H3 finger with W100 would have to undergo a conformational change from the current orientation observed in the 3B3 structure to the position seen in the b12-gp120 complex structure, if that is indeed the position observed in the 3B3-gp120 complex (future studies). In the 3B3 unbound structure, the indole side chain of W100 sterically clashes with the *N*-acetylglucosamine moiety of gp120. The early chain shuffling and phage display mutagenesis studies of b12 that evolved the sequence of 3B3 clearly demonstrated a preference for a Trp at position 98 in CDR-H3 over a Tyr.[12,16] The 3B3 Fab was selected over other Fabs with an approximately eightfold higher binding affinity over b12 for monomeric gp120s and ~5- to 54-fold enhancement in neutralization activity to b12 to various presumably trimeric gp120 molecules of primary isolates.[12] Subsequent CDR walking phage display experiments demonstrated a clear preference for the Glu-Trp-Gly sequence for positions 97–99 as seen in 3B3.[21] The side chain of E97 of 3B3 may form a hydrogen bond with the S365 side chain of gp120 (current distance is 2.0 Å). The replacement of Y98 of b12, which forms a hydrogen bond with R419 Nη1 of gp120, with a Trp in 3B3 may enhance binding affinities/neutralization abilities through more favorable van der Waals and hydrophobic interactions among the W98 indole side chain and residues P369, V372, and T373 of gp120. The selection of G99 in 3B3 presumably allows for more flexibility in this region for W98 and W100 to adopt conformations that would maximize binding interactions with gp120 (part of the "ligand-induced" binding mechanism of 3B3). Mutagenesis studies using the N31H, Q100eY 3B3 scFv immunotoxin architecture and reverting the Glu-Trp-Gly of 3B3 to the Pro-Tyr-Ser as seen in b12 displayed no changes in neutralization abilities to a zero- to sevenfold higher binding affinity changes to varying gp120s.[13] Nevertheless, a significant structural change most likely occurs from the unbound 3B3 state to the 3B3-gp120 bound structure.

At the C-terminal end of the CDR-H3, a point mutation of a Tyr has been introduced at Q100e in this variant of 3B3 reported here. The original sequences of b12 and 3B3 contained a Gln at position 100e of

the CDR-H3. Phage display mutagenesis studies randomizing residues at position 100e indicated a clear preference for an aromatic residue of either a Phe or a Tyr with approximately equal distribution.[21] Single point mutations of the 3B3 scFv with Q100e to a Tyr, Phe, and Trp had inhibitions at 50% levels (IC_{50}) of 9-, 6-, and 14-fold increase over wt-3B3 scFv (IC_{50} = 5.7 ng mL^{-1}), respectively.[13] Q100e in the b12-gp120 complex structure forms essentially no intermolecular contacts with the gp120 surface (only 5 $Å^2$ of surface area buried). In both b12 structures, Q100e Oε1 forms an intramolecular hydrogen bond to the nitrogen backbone of A93 CDR-L3 at the V_H-V_L interface (Fig. 6). The Q100eY mutation in the 3B3 structure disrupts this intramolecular hydrogen bond and most likely leads to a higher hydrophobic stabilization of the V_H-V_L interface with an aromatic side chain. In addition, the side chain of Q100eY of 3B3 could potentially form a new intermolecular hydrogen bond with K432 Nζ of gp120 (currently 4.3 Å away) accounting for some of the increased binding affinity/neutralization ability over the original 3B3 sequence. However, we speculate that the stabilization of the V_H-V_L interface contributes the majority to the increased neutralization levels, because enhancement values were observed with other aromatic residues of Phe or Trp, though not as high as with a Tyr at position 100e.[13] Future studies will dive deeper into the structural changes triggered by Q100eY mutation in 3B3.

The Q100eY mutation in the 3B3 structure causes a loop conformational change of the CDR-L3 relative to the b12 structures. Of significance, the b12-gp120 complex structure showed for the first time an antibody–antigen interface involving only residues of the CDRs of the V_H domain (Figs. 5 and 6). The regions around the loops of CDR-L3 and H3 in the b12 structures indicate a more solvent accessible surface and less packing efficiency compared with the 3B3 structure. Calculations of accessible surface area between 3B3 and b12 structures display a general trend of the CDR-L3 residues of b12 being more solvent accessible than 3B3 with the exception of G92 and S95 (Table III). The shape complementarity (S_c) of the V_H-V_L interfaces displays similar values of 0.74 and 0.72 for b12 bound and 3B3, respectively.[29] In the b12-gp120 complex structure, a water molecule (Wat17) forms four hydrogen bonds between atoms of CDR-L3, Q100e, and β-sheet V_H residues of W50 and E58 (Fig. 6). On the other hand, flipping of peptide bonds of G92 and A93 seen in the 3B3 structure triggered by the Q100eY mutation results in the removal of water in this region and allows for direct hydrogen bonding between main chain to main chain and main chain to side chain atoms at the V_H-V_L interface. Studies have demonstrated the importance of packing efficiency of the V_H-V_L antibody interface with correlations with antigen binding affinities.[28,30,31] We should point out these studies focused on antibody–antigen systems that used residues of both V_H and V_L CDR paratopes involved directly with bound antigens. Of course, we presume that 3B3 uses only heavy-chain residues as its parent molecule, b12, with its interaction with gp120. This will be clarified with the structure determination of the 3B3-gp120 complex. In the constant battle of generating NAbs against HIV, remarkable novel structural and mechanistic solutions have emerged in antibody–antigen recognition.[17,24]

In conclusion, we have determined the crystal structure of a N31H, Q100eY-3B3 scFv, an enhanced broadly NAb to the gp120 envelope protein of HIV. Structural comparisons of 3B3 with the unbound and bound structures of b12 indicate one of the largest conformational changes is CDR-H3 where the sequence evolved during phage display mutagenesis. The CDR-H3 of 3B3 may undergo a "ligand-induced" conformational change binding mechanism when bound with gp120. This is in contrast to the b12 structures, which show a preorganized CDR-H3 topology before gp120 interaction typical of a "lock-and-key" binding mechanism. A surprising feature of the 3B3 structure involves the change in loop conformation of CDR-L3 in comparison with the b12 structures. The 3B3 CDR-L3 loop conformation change was initiated by the single point mutation of Q100eY, a residue on the periphery of the b12-gp120 interface. The broadly NAb, b12 and siblings similar to 3B3, are the only antibodies to demonstrate engaging an antigen solely using variable heavy-chain residues of the CDR loops. The results presented here suggest that future affinity maturation of heavy chain only antibodies to HIV may be achieved by evolving framework residues at the V_H-V_L interface as have been observed in other antibody–antigen systems that use all CDR residues in antigen molecular recognition.

Materials and Methods

Protein expression and purification

The N31H, Q100eY 3B3 scFv gene[13] was synthesized using human codon optimization by Retrogen (San Diego, CA) and cloned into an AAV vector plasmid (pAAV.CMV.3B3). For bacterial expression, the 3B3 gene was then subcloned using unique Nco I and Not I restriction sites into a custom alkaline phosphatase expression vector containing a custom signal sequence for transport into the periplasm. A six-residue polyhistidine tag (His-Tag) was included after the signal sequence and before the starting amino acid of 3B3. The 3B3 vector was transformed into *E. coli* cell line BL21 CodonPlus RP (Stratagene) for expression. Cells were grown for 24 h using a low phosphate minimal media at 29°C as described previously.[32]

Isolation of the periplasmic proteins was performed using methods described previously.[32] Briefly, the *E. coli* cells (1 L of culture) were pelleted and frozen overnight at −80°C. The cell pellets were

resuspended with 4 mL of 0.1*M* sodium phosphate (pH 7.2), 0.15*M* NaCl buffer and incubated on ice for 30 min with constant shaking. Removal of the outer membranes involved a freeze-thaw procedure by placement of the resuspended pellets at −80°C for 1 h and thawing the frozen pellets in ambient temperature water with constant shaking. After centrifugation at 15,000 rpm for 30 min, the supernatant was removed for further purification.

3B3 was purified to homogeneity using protein L affinity chromatography media (Pierce). The supernatant was applied to a 2 mL bed volume of protein L affinity resin previously equilibrated with five bed volumes of binding buffer, 0.1*M* sodium phosphate, pH 7.2, 0.15*M* sodium chloride, at 4°C. After loading the supernatant through the column by gravity flow, the column was further washed with 10 bed volumes of binding buffer. Bound 3B3 was eluted from the protein L column using five bed volumes of elution buffer, 0.1*M* glycine, pH 2.5. The pH of the purified 3B3 was immediately neutralized with the addition of 1 mL of 1*M* of Tris-HCl, pH 9. SDS-PAGE gel electrophoresis indicated that 3B3 was >95% pure after protein L affinity chromatography. Protein concentration was determined using an extinction coefficient at 280 nm of 56.7 mM^{-1} cm^{-1}.[33] 3B3 protein yields were 1.4 mg L^{-1} culture.

Protein crystallization, data collection, structure determination, and refinement

For crystallization screening, the buffer of 3B3 was changed to 10 m*M* Tris-HCl, pH 7.5, and concentrated to 5.1 mg mL^{-1}. Sparse matrix crystal screening was performed using crystallization kits from Emerald Biosystems (Wizard Screens I, II, and III) at 19°C. Sitting drop vapor diffusion trials employed using 0.5 mL of each reservoir solution with a drop of 1 μL 3B3 and 1 μL of the reservoir solution. Hexagonal- and trigonal-shaped crystals grew from 20% (w/v) PEG-8000, 0.1*M* MES (pH 6.0), and 0.2*M* calcium acetate. Crystals were flash-frozen in liquid nitrogen by slowly increasing the glycerol concentration to 20% containing the reservoir solution.

X-ray diffraction data were collected at the General Medicine and Cancer Institutes Collaborative Access Team (GM/CA-CAT) beamline 23ID-D, Advanced Photon Source (APS), Argonne National Laboratories, Chicago, IL. The X-ray beam was collimated to an area between 5 and 300 μm^2 and diffraction data recorded with a MARmosaic 300 CCD detector at 100 K. X-ray diffraction data were collected with 2 s exposures for 0.25° oscillations for a total of 180° at a wavelength of 1.0332 Å with the detector distance at 350 mm. Data were integrated and scaled using HKL-2000.[34] X-ray data collection statistics are presented in Table I.

The crystal structure of 3B3 was phased using molecular replacement using only the variable heavy and light chains of b12 (2ny7.pdb[10]) as the search model using the program Phaser[20] within the Phenix package.[35] Six copies were located within the asymmetric unit with *Z*-scores of 9.7, 9.4, 10.4, 10.7, 9.6, and 12.6 for the resolution range of 30–3.5 Å. Data were phase extended to 2.5 Å and automatic model building performed using Resolve.[36] Before starting structure refinement, 10% of the data were randomly selected for R_{free} calculation. Simulated annealing torsional angle dynamics, conjugate gradient energy minimization, an overall anisotropic temperature factor and bulk solvent correction, and individual *B*-factor refinement were performed using phenix.refine.[35] NCS restraints were not used during any stage of structure refinement. Coot was used for model building.[37] Molprobity,[38] programs within CCP4,[39] and Pisa[40] were used for structural validation and analysis. All structural figures were generated using PyMOL (http://pymol.sourceforge.net). The coordinates have been deposited into the Protein Data Bank under accession code 3JUY.

Acknowledgment

X-ray data were collected using the National Institutes of Health GM/CA 23ID beamline at the Advanced Photon Source at Argonne National Laboratory, which is operated by UChicago Argonne, LLC, for the U.S. Department of Energy, Office of Biological and Environmental Research under contract DE-AC02-06CH11357. The authors thank Dr. Michael Becker and Dr. Nagarajan Venugopalan of the GM/CA staff for their assistance.

References

1. Cohen J (2007) AIDS research. Did Merck's failed HIV vaccine cause harm? Science 318:1048–1049.
2. Lewis AD, Chen R, Montefiori DC, Johnson PR, Clark KR (2002) Generation of neutralizing activity against human immunodeficiency virus type 1 in serum by antibody gene transfer. J Virol 76:8769–8775.
3. Johnson PR, Schnepp BC, Zhang J, Connell MJ, Greene SM, Yuste E, Desrosiers RC, Clark KR (2009) Vector-mediated gene transfer ejenders long-lived neutralizing activity and protection against SIV infeciton in monkeys. Nat Med 15:901–906.
4. Haynes BF, Montefiori DC (2006) Aiming to induce broadly reactive neutralizing antibody responses with HIV-1 vaccine candidates. Expert Rev Vaccines 5: 579–595.
5. Burton DR, Barbas CF, III, Persson MA, Koenig S, Chanock RM, Lerner RA (1991) A large array of human monoclonal antibodies to type 1 human immunodeficiency virus from combinatorial libraries of asymptomatic seropositive individuals. Proc Natl Acad Sci USA 88: 10134–10137.
6. Kwong PD, Wyatt R, Robinson J, Sweet RW, Sodroski J, Hendrickson WA (1998) Structure of an HIV gp120 envelope glycoprotein in complex with the CD4 receptor and a neutralizing human antibody. Nature 393:648–659.
7. Poignard P, Saphire EO, Parren PW, Burton DR (2001) gp120: biologic aspects of structural features. Annu Rev Immunol 19:253–274.

8. Zwick MB, Kelleher R, Jensen R, Labrijn AF, Wang M, Quinnan GV, Jr, Parren PW, Burton DR (2003) A novel human antibody against human immunodeficiency virus type 1 gp120 is V1, V2, and V3 loop dependent and helps delimit the epitope of the broadly neutralizing antibody immunoglobulin G1 b12. J Virol 77:6965–6978.
9. Zwick MB, Parren PW, Saphire EO, Church S, Wang M, Scott JK, Dawson PE, Wilson IA, Burton DR (2003) Molecular features of the broadly neutralizing immunoglobulin G1 b12 required for recognition of human immunodeficiency virus type 1 gp120. J Virol 77:5863– 5876.
10. Zhou T, Xu L, Dey B, Hessell AJ, Van Ryk D, Xiang SH, Yang X, Zhang MY, Zwick MB, Arthos J, Burton DR, Dimitrov DS, Sodroski J, Wyatt R, Nabel GJ, Kwong PD (2007) Structural definition of a conserved neutralization epitope on HIV-1 gp120. Nature 445:732–737.
11. Binley JM, Wrin T, Korber B, Zwick MB, Wang M, Chappey C, Stiegler G, Kunert R, Zolla-Pazner S, Katinger H, Petropoulos CJ, Burton DR (2004) Comprehensive cross-clade neutralization analysis of a panel of anti-human immunodeficiency virus type 1 monoclonal antibodies. J Virol 78:13232–13252.
12. Barbas CF, III, Hu D, Dunlop N, Sawyer L, Cababa D, Hendry RM, Nara PL, Burton DR (1994) In vitro evolution of a neutralizing human antibody to human immunodeficiency virus type 1 to enhance affinity and broaden strain cross-reactivity. Proc Natl Acad Sci USA 91: 3809–3813.
13. McHugh L, Hu S, Lee BK, Santora K, Kennedy PE, Berger EA, Pastan I, Hamer DH (2002) Increased affinity and stability of an anti-HIV-1 envelope immunotoxin by structure-based mutagenesis. J Biol Chem 277:34383–34390.
14. Saphire EO, Parren PW, Pantophlet R, Zwick MB, Morris GM, Rudd PM, Dwek RA, Stanfield RL, Burton DR, Wilson IA (2001) Crystal structure of a neutralizing human IGG against HIV-1: a template for vaccine design. Science 293:1155–1159.
15. Saphire EO, Montero M, Menendez A, van Houten NE, Irving MB, Pantophlet R, Zwick MB, Parren PW, Burton DR, Scott JK, Wilson IA (2007) Structure of a high-affinity "mimotope" peptide bound to HIV-1-neutralizing antibody b12 explains its inability to elicit gp120 cross-reactive antibodies. J Mol Biol 369:696–709.
16. Barbas CF, III, Collet TA, Amberg W, Roben P, Binley JM, Hoekstra D, Cababa D, Jones TM, Williamson RA, Pilkington GR, Haigwood NL, Cabezas E, Satterthwait AC, Sanz I, Burton DR (1993) Molecular profile of an antibody response to HIV-1 as probed by combinatorial libraries. J Mol Biol 230:812–823.
17. Kwong PD, Wilson IA (2009) HIV-1 and influenza antibodies: seeing antigens in new ways. Nat Immunol 10: 573–578.
18. Johnson PR, Schnepp BC, Connell MJ, Rohne D, Robinson S, Krivulka GR, Lord CI, Zinn R, Montefiori DC, Letvin NL, Clark KR (2005) Novel adeno-associated virus vector vaccine restricts replication of simian immunodeficiency virus in macaques. J Virol 79:955–965.
19. Ruiz N, Kahne D, Silhavy TJ (2006) Advances in understanding bacterial outer-membrane biogenesis. Nat Rev Microbiol 4:57–66.
20. McCoy AJ, Grosse-Kunstleve RW, Adams PD, Winn MD, Storoni LC, Read RJ (2007) Phaser crystallographic software. J Appl Crystallogr 40:658–674.
21. Yang WP, Green K, Pinz-Sweeney S, Briones AT, Burton DR, Barbas CF, III (1995) CDR walking mutagenesis for the affinity maturation of a potent human anti-HIV-1 antibody into the picomolar range. J Mol Biol 254:392–403.
22. Al-Lazikani B, Lesk AM, Chothia C (1997) Standard conformations for the canonical structures of immunoglobulins. J Mol Biol 273:927–948.
23. Kuroda D, Shirai H, Kobori M, Nakamura H (2009) Systematic classification of CDR-L3 in antibodies: implications of the light chain subtypes and the VL-VH interface. Proteins 75:139–146.
24. Burton DR, Stanfield RL, Wilson IA (2005) Antibody vs. HIV in a clash of evolutionary titans. Proc Natl Acad Sci USA 102:14943–14948.
25. Darbha R, Phogat S, Labrijn AF, Shu Y, Gu Y, Andrykovitch M, Zhang MY, Pantophlet R, Martin L, Vita C, Burton DR, Dimitrov DS, Ji X (2004) Crystal structure of the broadly cross-reactive HIV-1-neutralizing Fab X5 and fine mapping of its epitope. Biochemistry 43:1410–1417.
26. Huang CC, Tang M, Zhang MY, Majeed S, Montabana E, Stanfield RL, Dimitrov DS, Korber B, Sodroski J, Wilson IA, Wyatt R, Kwong PD (2005) Structure of a V3-containing HIV-1 gp120 core. Science 310:1025–1028.
27. Zwick MB, Bonnycastle LL, Menendez A, Irving MB, Barbas CF, III, Parren PW, Burton DR, Scott JK (2001) Identification and characterization of a peptide that specifically binds the human, broadly neutralizing anti-human immunodeficiency virus type 1 antibody b12. J Virol 75:6692–6699.
28. Sundberg EJ, Mariuzza RA (2002) Molecular recognition in antibody-antigen complexes. Adv Protein Chem 61: 119–160.
29. Lawrence MC, Colman PM (1993) Shape complementarity at protein/protein interfaces. J Mol Biol 234: 946–950.
30. Pellequer JL, Chen S, Roberts VA, Tainer JA, Getzoff ED (1999) Unraveling the effect of changes in conformation and compactness at the antibody V(L)-V(H) interface upon antigen binding. J Mol Recognit 12:267–275.
31. Masuda K, Sakamoto K, Kojima M, Aburatani T, Ueda T, Ueda H (2006) The role of interface framework residues in determining antibody V(H)/V(L) interaction strength and antigen-binding affinity. FEBS J 273:2184–2194.
32. Walsh ST, Jevitts LM, Sylvester JE, Kossiakoff AA (2003) Site2 binding energetics of the regulatory step of growth hormone-induced receptor homodimerization. Protein Sci 12:1960–1970.
33. Pace CN, Vajdos F, Fee L, Grimsley G, Gray T (1995) How to measure and predict the molar absorption coefficient of a protein. Protein Sci 4:2411–2423.
34. Otiwinowski Z, Minor W,Processing of X-ray diffraction data collected in oscillation mode. In: Carter CWJ,Sweet RM, Eds. (1997) Methods in enzymology, Vol.276.New York:Academic Press, 307–326.
35. Zwart PH, Afonine PV, Grosse-Kunstleve RW, Hung LW, Ioerger TR, McCoy AJ, McKee E, Moriarty NW, Read RJ, Sacchettini JC, Sauter NK, Storoni LC, Terwilliger TC, Adams PD (2008) Automated structure solution with the PHENIX suite. Methods Mol Biol 426:419–435.
36. Terwilliger TC (2003) SOLVE and RESOLVE: automated structure solution and density modification. Methods Enzymol 374:22–37.
37. Emsley P, Cowtan K (2004) Coot: model-building tools for molecular graphics. Acta Crystallogr D 60:2126–2132.
38. Davis IW, Leaver-Fay A, Chen VB, Block JN, Kapral GJ, Wang X, Murray LW, Arendall WB, III, Snoeyink J, Richardson JS, Richardson DC (2007) MolProbity: all-atom contacts and structure validation for proteins and nucleic acids. Nucleic Acids Res 35 (Web Server issue): W375–W383.
39. Collaborative Computational Project, No. 4(1994) The CCP4 suite: programs for protein crystallography. Acta Crystallogr D 50:760–763.
40. Krissinel E, Henrick K (2007) Inference of macromolecular assemblies from crystalline state. J Mol Biol 372: 774–797.